

Investigation of convective-conductive heat transfer in geothermal system

P. Jalili^a, D.D. Ganji^{a,*}, S.S. Nourazar^b

^a Department of Mechanical Engineering, Babol Noshirvani University of Technology, Babol, Iran

^b Department of Mechanical Engineering, Amirkabir University of Technology, Tehran, Iran



ARTICLE INFO

Keywords:

Borehole heat exchangers
Numerical method
Heat transfer processes
Geothermal energy
Finite volume analysis

ABSTRACT

Geothermal energy is one of the well-known types of renewable energies that can be considered as a promising alternative to fossil fuels in order to mitigate the CO₂ emission in atmosphere. Geothermal energy has recently been used for heating and cooling systems in many countries of the world. Therefore, studying such kind of energy seems important and necessary. This paper studies the heat transfer processes in a borehole heat exchanger (BHE). The flow of fluid in a BHE has been considered with different geometries and heat transfer processes are modeled numerically and in a finite volume method through convection and conductivity. First, a single U-shaped BHE was modeled and its thermal properties were investigated and then other geometries were studied to obtain the best geometry and heat transfer efficiency. In order to increase the heat transfer in the inner part of the pipes, the fin with the given specifications was used and the modeling was carried out and the thermal parameters were compared for three BHE's with different geometries. In the final part, optimization results are presented, and the interaction of parameters on the Nusselt number and friction coefficient have been investigated. Also, the desirability of optimization and reliability is given to the results presented in percentage terms. Comparing the results of this article with the results of previous research shows a very good agreement and therefore the applied method is reliable and accurate.

Introduction

Fossil fuels mortality, diversification into energy sources, sustainable development and energy security and environmental problems caused by the use of fossil fuels on the one hand and clean and renewable sources of new energy such as the sun, wind and geothermal on the other hand has caused the world's attention to develop and expand use of renewable energy and increase the share of those resources in the global energy basket. Geothermal energy means energy from the internal origin of the earth. This energy emanates from the inner part of the earth, in the form of tangible heat and there are rocks and water in the gaps and pores inside the rock in the earth's crust. Over the life of the earth, this internal heat is slowly produced and kept within the ground. This has made it an important source of energy and is now being considered as a new energy source.

In geothermal systems, geothermal wells and heat pumps are commonly known as geothermal Borehole Heat Exchanger (BHE). To design geothermal BHEs, the thermal conductivity of the earth and the thermal resistance of the well are required. Usually, the above parameters are estimated using the experimental Thermal Response Test (TRT) which for first time was proposed by Mogensen [1]. Subsequently, supplementary guides of the TRT are suggested by Ashrae [2] and Sanner et al. [3].

The topic of geothermal heat pumps has attracted much attention as a renewable energy technology and has been used for heating and cooling [4–6]. Recent studies have been conducted to study the efficiency of geothermal heat pump systems [7–9]. Li et al. [10] experimentally investigated the efficiency of a U-shaped vertical BHE in which, temperature changes and thermal equilibrium of the system have been numerically simulated and analyzed. Those results indicated that the geothermal source could be used as a fountain or thermal well for the geothermal heat pump system to achieve higher returns and more energy storage.

Karabacak et al. [11] investigated the cooling performance of the geothermal heat pump system in Denizli, Turkey experimentally. They accurately showed that the relations of the coefficients of operation of the geothermal heat pump were proportional to the weathering information, including solar radiation, wind speed, relative humidity and external temperature. Michopoulos et al. [12,13] studied the performance of a system installed in Greece for heating and cooling. Ozyurt et al. [14] experimentally studied the performance of vertical geothermal heat pumps for the assessment of cold weather in Turkey and the coefficient of heat pump performance and system performance were calculated. Hwang et al. [15] examined the cooling performance of the geothermal heat pump system installed in the building of a school in

* Corresponding author.

E-mail address: ddg_davood@yahoo.com (D.D. Ganji).

<https://doi.org/10.1016/j.rinp.2018.06.047>

Received 17 May 2018; Received in revised form 15 June 2018; Accepted 19 June 2018

Available online 11 July 2018

2211-3797/ © 2018 The Authors. Published by Elsevier B.V. This is an open access article under the CC BY license

(<http://creativecommons.org/licenses/by/4.0/>).

Nomenclature

g	Grout
L	Borehole depth
u	Refrigerant velocity
ρ	Fluid density
c	Specific heat of the fluid
λ	Fluid thermal conductivity
λ_g	Grout thermal conductivity
c_g	Grout specific thermal capacity

$b_{\alpha\beta}$	Thermal coefficient between two components
f	coefficient of friction
P	stepping of Fin
Nu	Nusselt number
t	Pipe thickness
Re	Reynolds number
DR	Diameter rate
D	Distance of the center of the two pipes
d	Pipe diameter
d_g	Diameter of grout

South Korea. They discussed the system's performance and the effects of outdoor temperature. Li and colleagues [16] analyzed the thermal resistance of vertical U-shaped BHEs in the cold regions of China. They provided a new solution that reduced the thermal resistance of U-shaped BHEs and increased thermal efficiency. They considered the model once insulated and again without insulation at the bottom of the exhaust pipe and studied numerically. They examined the isolation effect of the tube on the outlet temperature, the soil temperature, and the heat transfer rate per unit length of the pipe.

Lei et al. [17] investigated the inhomogeneity of energy production under different working conditions in low dual enthalpy geothermal systems. They used finite element method to model fluid flow and heat transfer over time.

Crooijmans et al. [18] studied the thermal efficiency of a BHE with centrifugal tubes. They calculated the distribution of fluid temperature and investigated the effect of the discharge flow of the inlet fluid, as well as the effect of the filler materials on the fluid temperature.

BniLam et al. [19] simulated the heat transfer in a U-shaped BHE, and analyzed it analytically. They performed discretization in the time domain and studied the effect of friction at different flow rates and in different viscosities. Akbar et al. [20] studied numerically the unstable

flow of high enthalpy fluid in a geothermal BHE. They solved the governing equations with finite element method and investigated important physical phenomena along wells including phase change, compressibility and thermal interaction.

Regarding to the review of the research carrying out on the current subject matter and its applications in heating systems, electricity gen-

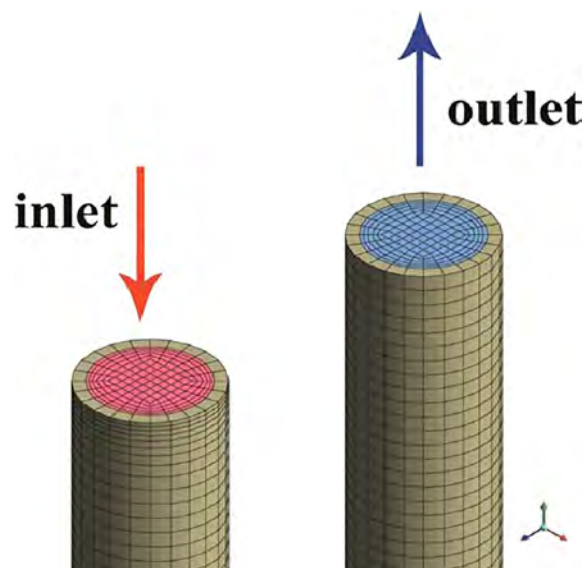


Fig. 2. Structured mesh used in the fluid and pipe area.

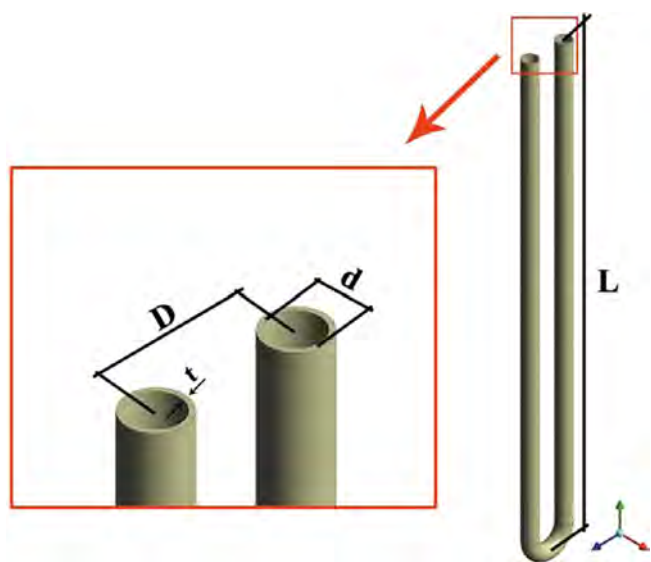


Fig. 1. U-type BHE geometry.

Table 1
U-type BHE dimensions.

Characteristic	Symbol	Size (mm)
Pipe Depth	L	1000
Inner pipe diameter	d	26
Distance of the center of the two pipes	$D = 3d$	78
Pipe thickness	t	2.9

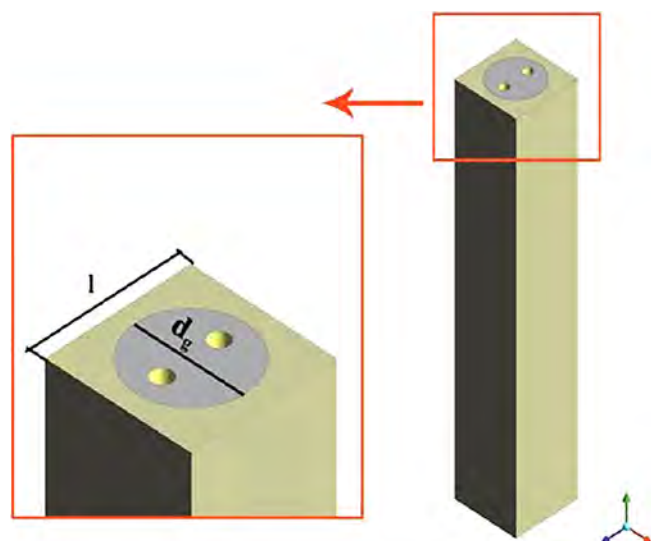


Fig. 3. Geothermal BHE, considering the parts of the grout and the surrounding soil.

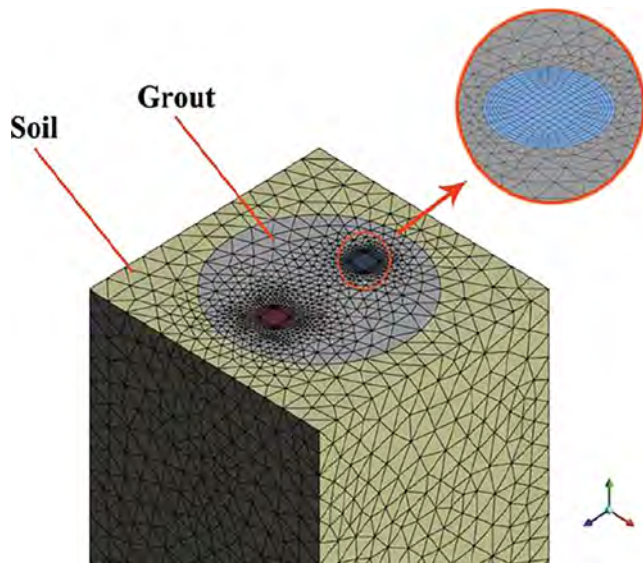


Fig. 4. Gridding of BHE, considering grout and surrounding soil.

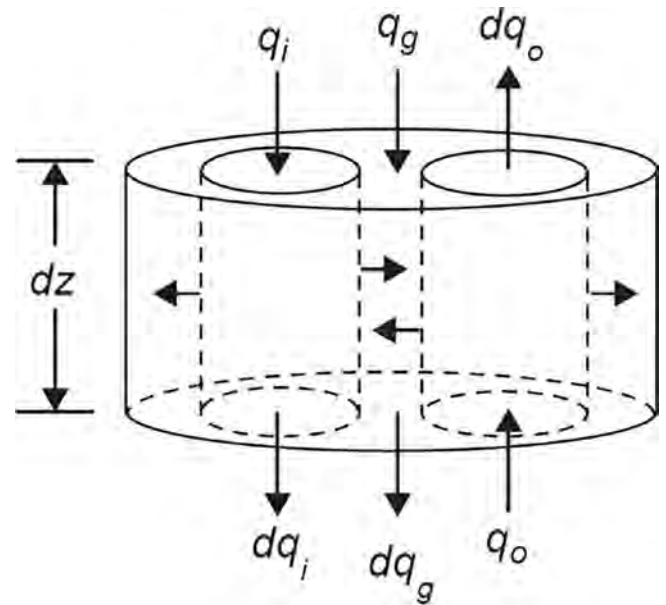


Fig. 6. Control volume of a single U-pipe BHE [21].

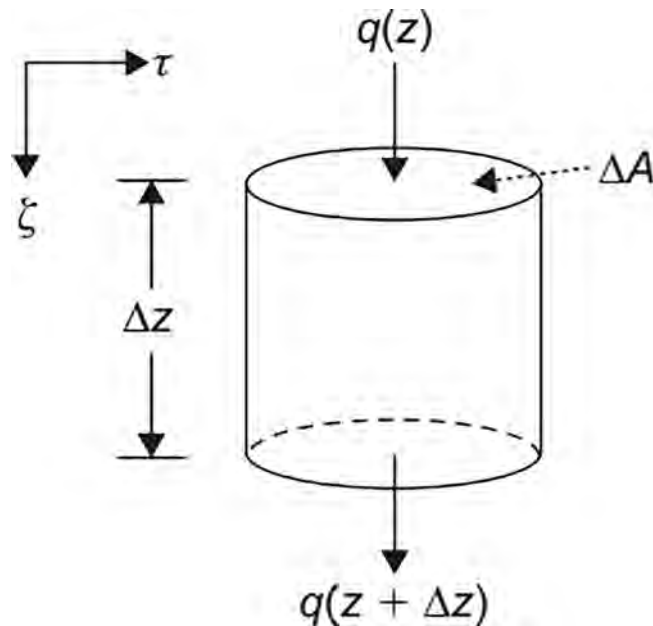


Fig. 5. Control volume of a single component [21].

eration, etc., in particular in recent years, the study of the process of heat transfer in the geothermal wells is necessary and important.

In this paper, following the mentioned works, temperature distribution along the U tube was investigated numerically by finite volume method. Even more, effect of tube different geometries was studied adequately in order to understand how those can influence on the enhancement of heat transfer progresses.

Methology

Geometry and physical model

The main part of a geothermal BHE is a U-shaped tube in which the fluid enters the pipe on one side and then passes through the tube and transfers heat to the other parts. The schematic of the tube is shown in Fig. 1 and the dimensions of the BHE are also given in the Table 1. For gridding of U-shaped pipe, structure mesh has been used. So, after gridding with the number of different cells and performing the mesh

Table 2

Physical properties of materials.

	$\rho C_p \left(\frac{J}{m^2k} \right)$	$k \left(\frac{w}{mk} \right)$	$\mu \text{ (ps.s)}$
Water	4.1298×10^6	0.38	0.0052
Pipe	2.2×10^6	0.42	-
Grout	1.69974×10^6	0.6	-
Soil	6.72×10^5	0.85	-

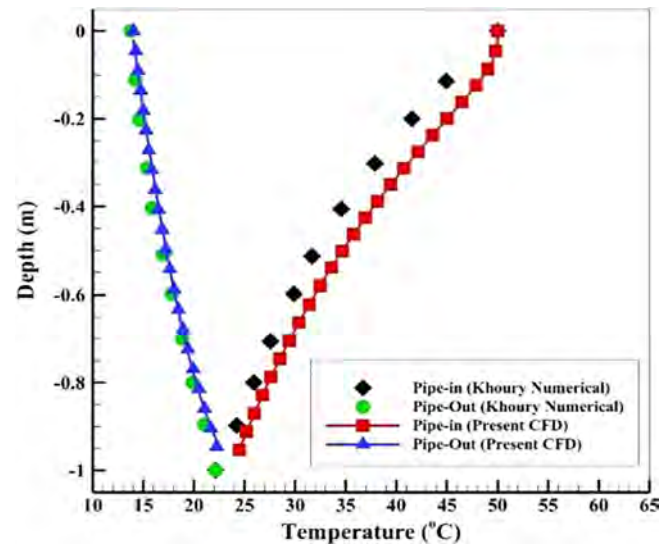


Fig. 7. Temperature distribution in pipe-in and pipe-out.

study according to the Nusselt number, a number of 434,335 cells were created for gridding, as shown in Fig. 2. In order to model geothermal wells, the distance between the U-pipe and the surrounding area is stuffed by the fill material, which is usually considered as a grout. Its modeling is shown in Fig. 3. The diameter of the grout d_g and the length of the soil l are also equal to 0.156 and 0.234 m respectively. The mesh in the pipe section, as in the previous state, has been structured and unstructured in the soil section that is shown in Fig. 4.

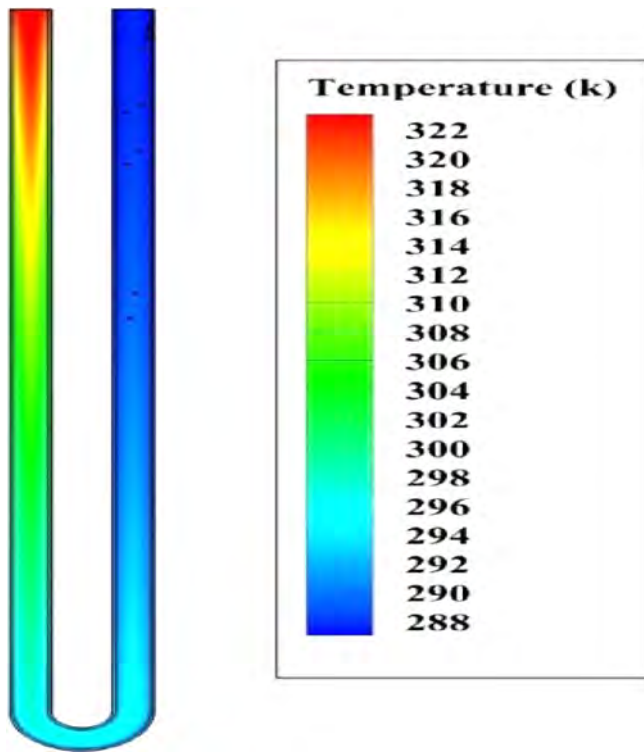


Fig. 8. Temperature distribution in U-type BHE.

Governing equations

A geothermal BHE consists of an inlet pipe, an outlet pipe and a filler material that each of them acts as a channel, which transmits heat in the axial direction and at the level of contact with other components. In this way, the components of the BHE can be considered as parallel pipes and generalized equations governing the parallel components for the desired BHE. In order to obtain the governing equations for parallel pipes, the governing equations on a pipe are first considered, and then the equations for parallel pipes are derived from those equations [21]. In a region, the heat equation is obtained by the laws of mass conservation and Fourier. According to the Fig. 5, the heat transfer rate cross to the surface in one dimension is:

$$q(z) = -\lambda \frac{\partial T(z, t)}{\partial z} \Delta A \tag{1}$$

That λ is thermal conductivity and T is the temperature. Not considering an external work, the amount of heat (internal energy) in the control volume at time is equal to:

$$H(t) = \rho c_p T(z, t) \Delta A \Delta z \tag{2}$$

which ρ is the mass density of the material and c_p is the specific heat capacity. According to the energy conversion law, with equal to above amounts and applying the mathematical rules [21], the transient heat conduction equation in one dimension is:

$$\rho c_p \frac{\partial T}{\partial t} - \lambda \frac{\partial^2 T}{\partial z^2} = 0 \tag{3}$$

If the convective heat transfer is also considered, the advection term should be considered. For this purpose, instead of the temperature derivative, we must consider the material derivative of temperature. After simplification of mathematical formulation, three dimensional heat fluxes are obtained as follows:

$$\rho c_p \frac{\partial T}{\partial t} + \text{div } q = 0 \tag{4}$$

in which

$$q = -\lambda \text{grad } T + \rho c_p u T \tag{5}$$

According to above equations, for single U pipe BHE (Fig. 6), governing equation can be obtained as below:

$$\rho c \frac{\partial T_i}{\partial t} - \lambda \frac{\partial^2 T_i}{\partial z^2} + \rho c u \frac{\partial T_i}{\partial z} = b_{ig}(T_i - T_g)$$

$$\rho c \frac{\partial T_o}{\partial t} - \lambda \frac{\partial^2 T_o}{\partial z^2} - \rho c u \frac{\partial T_o}{\partial z} = b_{og}(T_o - T_g)$$

$$\rho c_g \frac{\partial T_g}{\partial t} - \lambda_g \frac{\partial^2 T_g}{\partial z^2} = b_{ig}(T_g - T_i) + b_{og}(T_o - T_g)$$

With boundary and initial conditions:

$$T_i(z, 0) = T_o(z, 0) = T_g(z, 0) = T_s(z, 0)$$

$$T_i(0, t) = T_{in}(t)$$

$$T_i(L, 0) = T_o(L, 0) \text{ \& } q_i(L, 0) = q_o(L, 0)$$

$$\lambda_g \frac{\partial T_g(z, t)}{\partial z} = b_{gs}(T_g(z, t) - T_s(z, t)) \tag{6}$$

where g, i, and o refer to grout, pipe in and pipe out respectively. $b_{\alpha\beta}$ is thermal coefficient between component α and component β .

Heat transfer process was simulated in BHEs using computational fluid dynamics. Ansys Fluent software was used for simulations, and after validating the results, three different types of BHE were simulated. And finally, to improvement of heat transfer, the existing parameters optimized with the help of extensive levels. Fluent software uses a finite volume method to solve equations. Given the Reynolds number, the flow in all simulations is laminar. The boundary conditions in the inlet and outlet are velocity and atmospheric pressure, respectively. Walls have been assumed with constant temperature assumption, and the

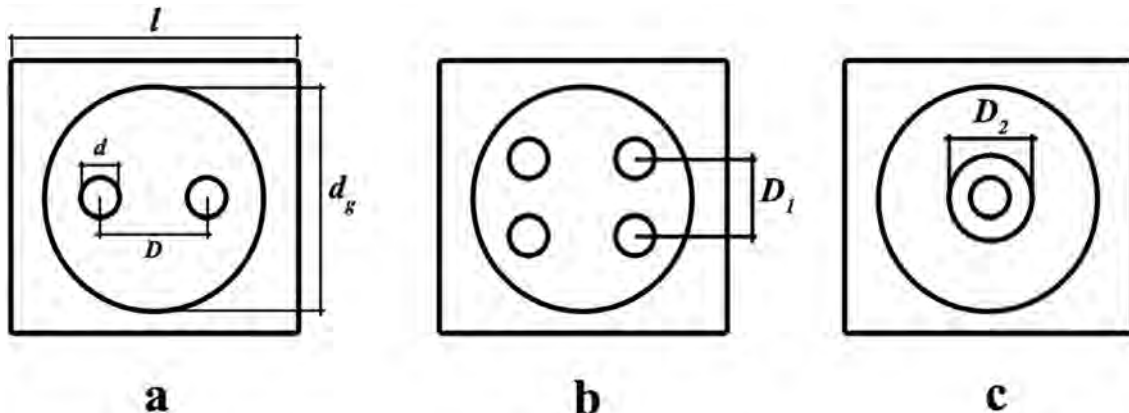


Fig. 9. Piping arrangement in three BHEs.

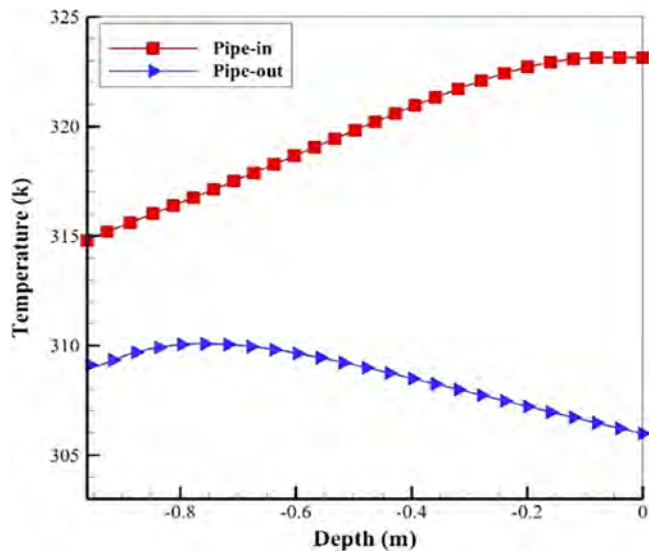


Fig. 10. Temperature distribution in the centerline of the pipe-in and pipe-out of case a.

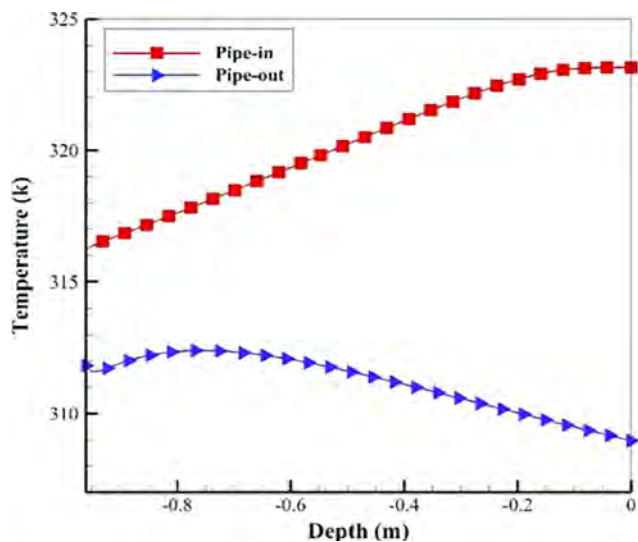


Fig. 11. Temperature distribution in the centerline of the pipe-in and pipe-out of case b.

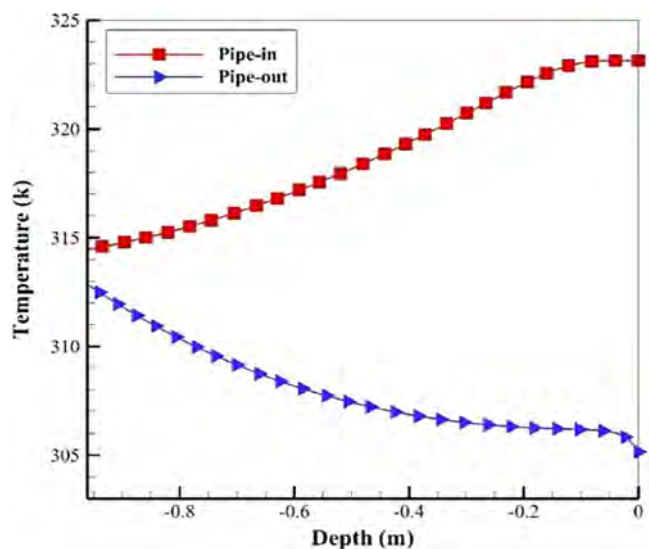


Fig. 12. Temperature distribution in the centerline of the pipe-in and pipe-out of case c.

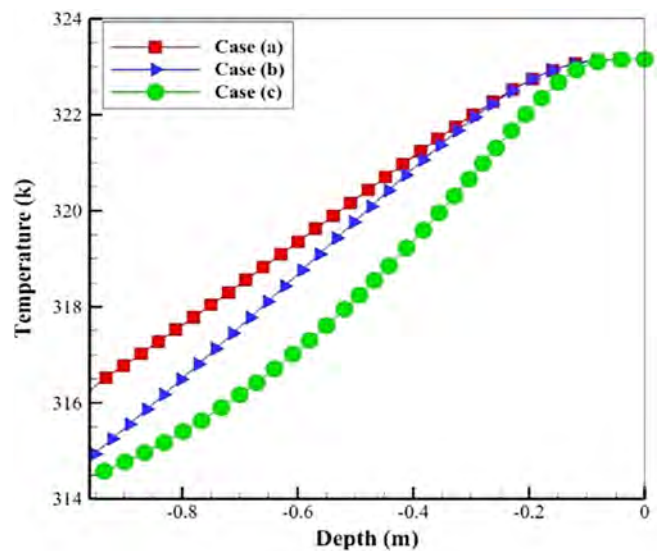


Fig. 13. Temperature distribution in the centerline of pipe-in for all three BHEs.

condition of convection has been used for validation and optimization. The physical properties of the materials used in Table 2 are presented.

Results and discussion

Single U-pipe

Borehole heat exchangers have been studied numerically by some researchers [22–25]. According to previous studies, most of them are on single U-type BHE. In this section, the simulations are performed on a single U-type BHE and then the results are validated with other investigations. The boundary conditions of the outer wall are placed in the form of forced convection heat transfer. For validation, the results of the Al-Khoury et al. [26] have been used. In which, conditions and physics of the flow have been similar to present study. The distribution of heat transfer in pipe-in and pipe-out is shown in Fig. 7. Also, Fig. 8 shows the temperature distribution in throughout U-type BHE.

Other geometries

In this section, single U-type BHE has been compared to other

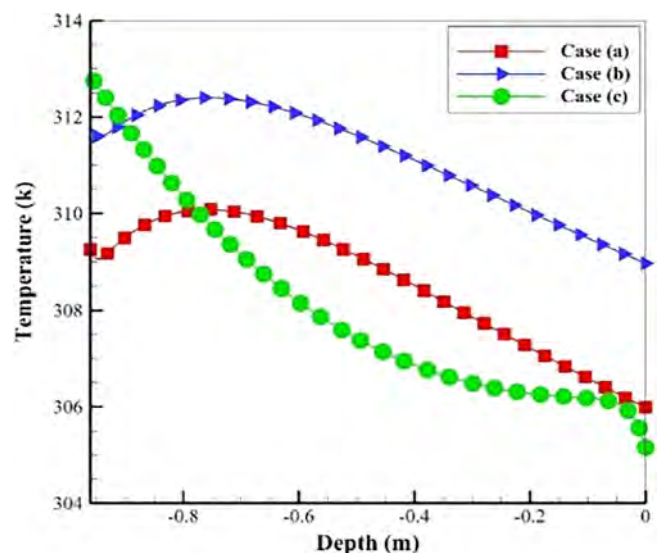


Fig. 14. Temperature distribution in the centerline of pipe-out for all three

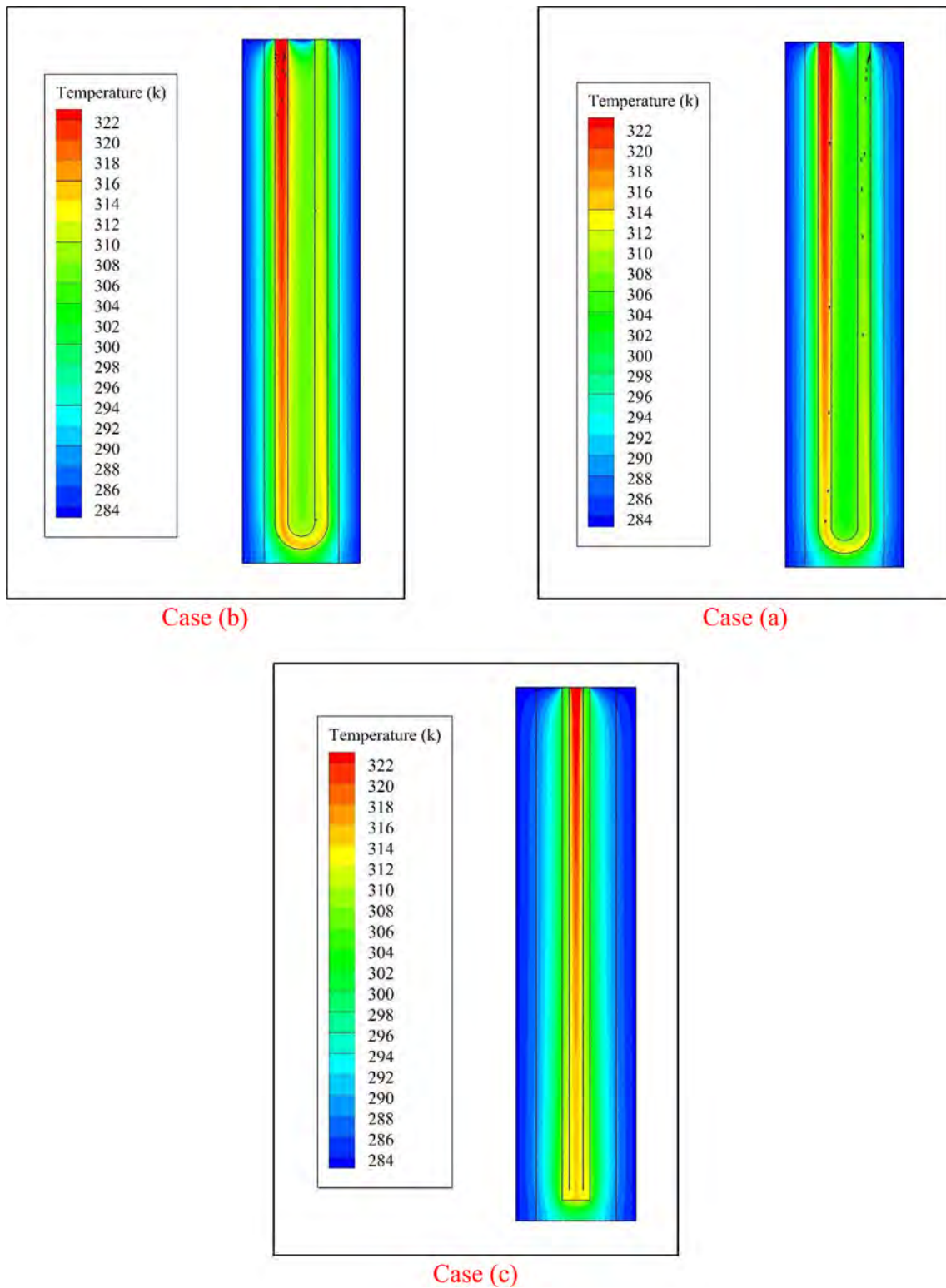


Fig. 15. Temperature contours in the central section of all three BHEs.

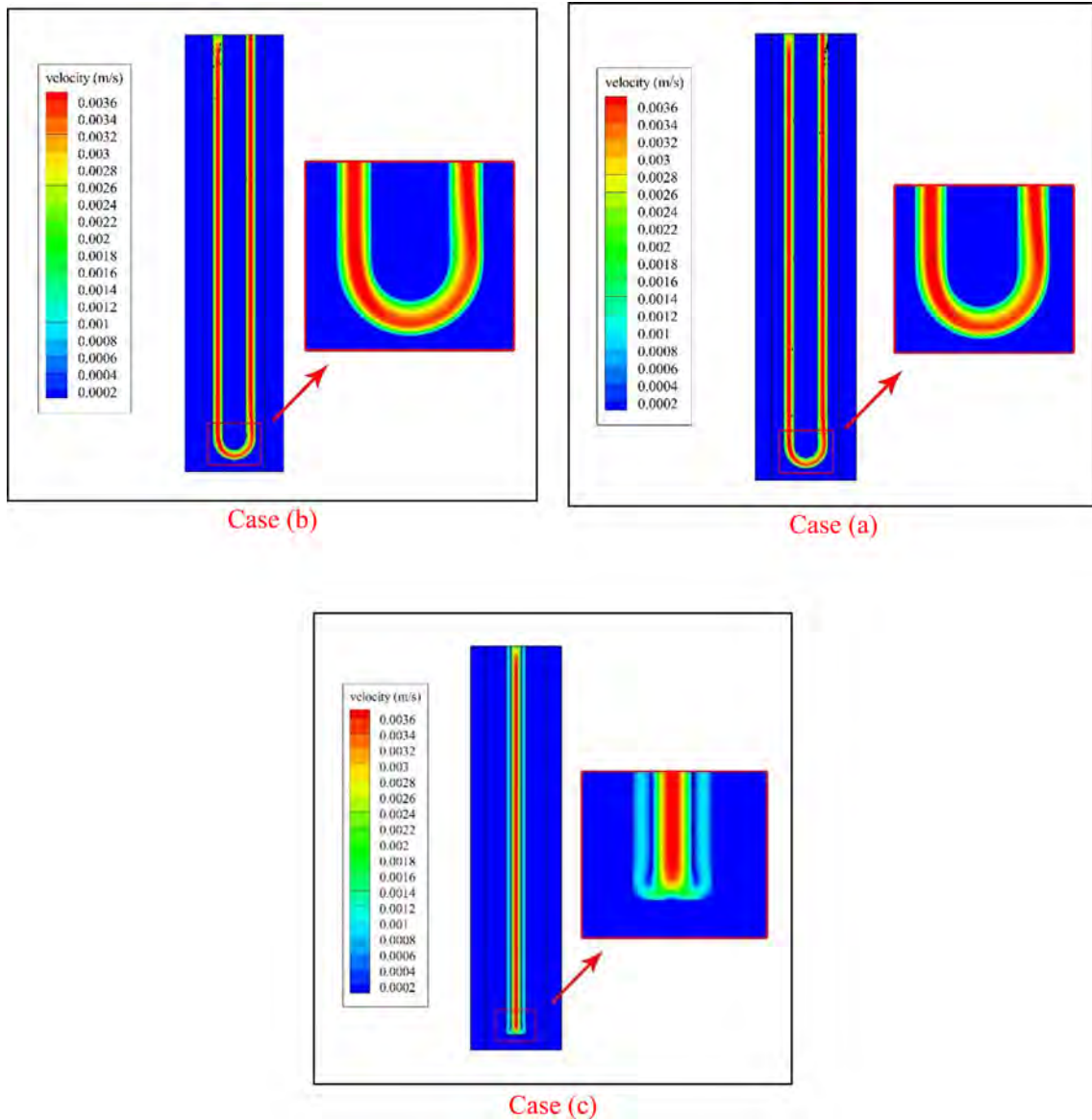


Fig. 16. Velocity contours in the central Section of all three BHE.

geometries that is shown in Fig. 9. In all three cases, the area of the soil is square with sides with length l , as well as the area of the grout in the form of a cylinder of diameter (d_g). In the Fig. 9 and case (a), the geometry is similar to the original one. In other words, case a is simulated. In case b, two U-shaped BHEs with dimensions similar to case a are considered. Also, case C is a BHE that the fluid enters from the central pipe and exits from outer circle with diameter of (D_2). In all three cases, the BHE depth is equal to 1 m. Relation between Dimensions of different cases is as below:

$$D = 3d, \quad d_g = 2D = 6d, \quad l = \frac{3}{2}d_g, \\ D_1 = 2d, \quad D_2 = 2d \quad (7)$$

The inlet temperature for water and the surrounding soil temperature are 50 °C and 10 °C. In Fig. 10, the temperature distribution for case a, is shown in the centerline of inlet pipe. Water is entered to the pipe with

Reynolds number of 50 and the temperature of 323.15°K. The output temperature for this model is about 306°K. In Fig. 11, the temperature distribution is shown in the centerline of the pipe-in and pipe-out of case b. In Fig. 11, water is entered at temperature of 323.15°K, and it is exited at temperature of about 309°K. In this case heat transfer between pipes and the another parts is less than case a, The water’s output temperature is higher than case a (Fig. 12).

The temperature distribution of the pipe-out for this case is slightly different from the previous two cases. This difference is due to the fact that the outlet fluid is heated by the inlet fluid and is cooled by the surrounding grout. In other words, the outlet fluid is exposed to the temperature of the surrounding grout as well as the inlet fluid. In the following, the temperature distribution in the centerline of pipe-in is given for all three BHEs.

As it can be seen in Fig. 13, the temperature in the centerline of the BHE of type a, and in the deep part is greater than the other two BHE’s,

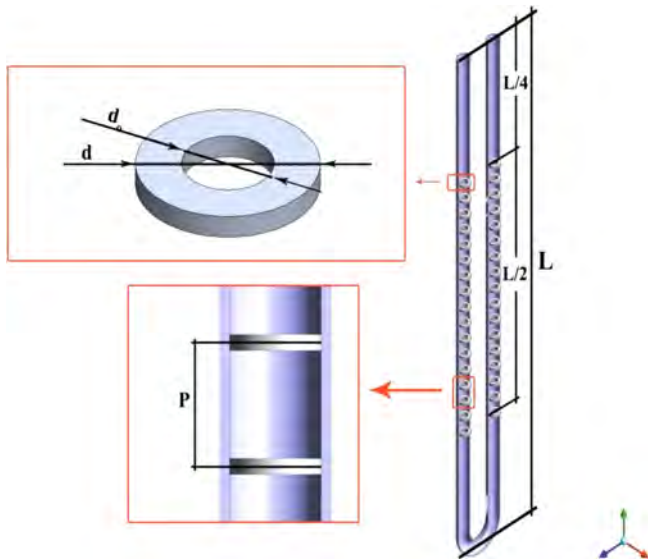


Fig. 17. Geometry of BHE with Fins and their location specifications.

Table 3
Simulation cases according to the parameters level.

Case No.	P	Re	DR
1	31.25	100	1.3
2	125	100	1.3
3	31.25	200	1.3
4	125	200	1.3
5	31.25	100	2
6	125	100	2
7	31.25	200	2
8	125	200	2
9	31.25	150	1.65
10	125	150	1.65
11	62.5	100	1.65
12	62.5	200	1.65
13	62.5	150	1.3
14	62.5	150	2
15	62.5	150	1.65

in other words, the fluid flow has lost less temperature than two other BHEs. While the BHE of type C lost more temperature in the input region so the fluid is colder than deep part.

In Fig. 14, the temperature distribution is shown in the centerline of pipe-out for all three BHEs. As it is shown, the output temperature of the c-type BHE is less than the other two types. In other words, heat transfer in this BHE is.

More than the other two types, so it has higher efficiency. The fluid in the output of this BHE is exposed to temperature gradients from the inlet fluid and the grout. Type (a) of BHE also has a cooler outlet temperature than the type (b). This is due to higher temperature gradients of this BHE than type (b). In BHE type (b), since two U-shaped pipes are used, the fluid in the output of this BHE is exited from the BHE with higher temperatures. In the following, the temperature contours are presented in all three BHEs. As it can be seen from Fig. 15, type (c) BHE has a lower output temperature than two other BHEs. Speed contours are also shown in Fig. 16.

Fin application in BHE

In order to enhance the heat transfer (EHT) in the BHE, the ring-shaped fins are used. The length of test section is half the length of the whole pipe. This area is located at a distance of one quarter of the length of the pipe from its beginning. In Fig. 17 fin geometry and location of the test section are shown. Here, effects of geometric parameters such as step (P) and the diameter rate of the rings (DR = d/d_o) and also Reynolds number on Nusselt number and surface friction are investigated. The Reynolds number is obtained from equation (8).

$$Re = \frac{\rho U D}{\mu} \tag{8}$$

Also, The Nusselt number is shown as bellow:

$$Nu = \frac{h D}{k} \tag{9}$$

and coefficient of friction is obtained from Eq. (10).

$$f = \frac{\Delta P}{\frac{\rho u^2 L}{2 D}} \tag{10}$$

In order to simulate and illustrate the fin influences on the EHT, Response Surface Methodology (RSM) based on Central Composite Design (CCD) is applied to obtain an optimization design for heat exchangers. Table 3 shows parameters level in CCD method. According to the test design technique, 15 different models for simulations are determined. Figures in Appendix show the contours of the maximum and minimum states of optimization parameters. These charts include contours of temperature, velocity, pressure and streamwises. In Fig. 18, contours of item number one of Table 3 are shown. The flow with Reynolds 100 enters the BHE, therefore, due to its speed, fluid has cooling time and temperature has dropped to about 4 °C in the output. Streamwises also indicate that fluid passes uniformly across the rings and maintains the apparent shape of the flow. The other cases (which are shown in Appendix) have been performed in order to obtain the optimize value of Nusselt and friction values which are listed in Table 4.

Optimization according to existing parameters

In this section, optimization results are presented, and the interaction of parameters on the Nusselt number and friction coefficient have been investigated. Finally, the desirability of optimization and reliability is given to the results presented in percentage terms. Also, quadratic relations are proposed for Nusselt number and friction coefficient according to design parameters. In this section, the interaction effect of design parameters on the Nusselt number and the coefficient of friction is discussed. In Fig. 19 the interactions of Reynolds number and the steps of the Fins on the Nusselt number are shown. It is known that as the Reynolds number increases, the Nusselt number also increases. This is true in laminar internal flow. While increasing the number of fins or, in other words, decreasing the step, it is seen that the Nusselt number decreases. In any case, the maximum number of Nusselt numbers will be obtained according to the graph shown when the Reynolds number is 200 and the Fins' steps is also about 100 mm. In this case, the best interaction mode of these two parameters is on the Nusselt number. Fig. 20 examines the parameters of the diameter rate and Reynolds number on the Nusselt number. As can be seen, increasing the diameter rate, or, in other words, increasing the fin thickness, the Nusselt number will increase. In other words, by

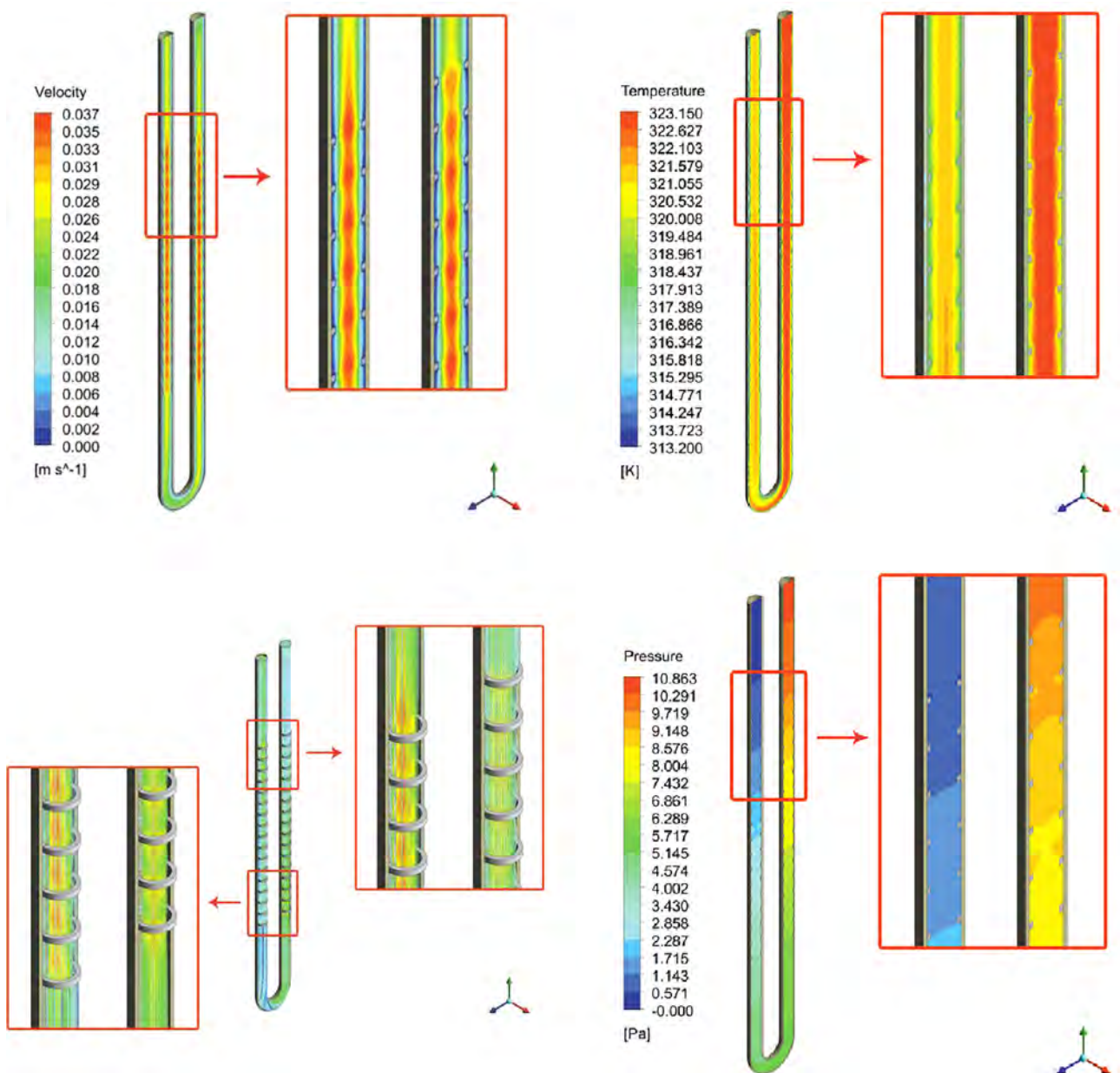


Fig. 18. Temperature, velocity, pressure and streamwise contours for case number 1.

Table 4
Nusselt values and surface friction coefficient for simulated cases.

Case No.	P	Re	DR	Nu	f
1	31.25	100	1.3	8.644407	1.016917
2	125	100	1.3	9.100598	0.817953
3	31.25	200	1.3	13.7456	0.577772
4	125	200	1.3	14.47312	0.459546
5	31.25	100	2	9.33323	4.29355
6	125	100	2	9.361461	2.706432
7	31.25	200	2	16.34737	2.982438
8	125	200	2	17.87414	2.383553
9	31.25	150	1.65	11.67012	1.571833
10	125	150	1.65	12.08593	1.063629
11	62.5	100	1.65	8.888791	1.752618
12	62.5	200	1.65	15.26382	1.187453
13	62.5	150	1.3	11.79241	0.638015
14	62.5	150	2	14.23553	3.063548
15	62.5	150	1.65	11.81342	1.341448

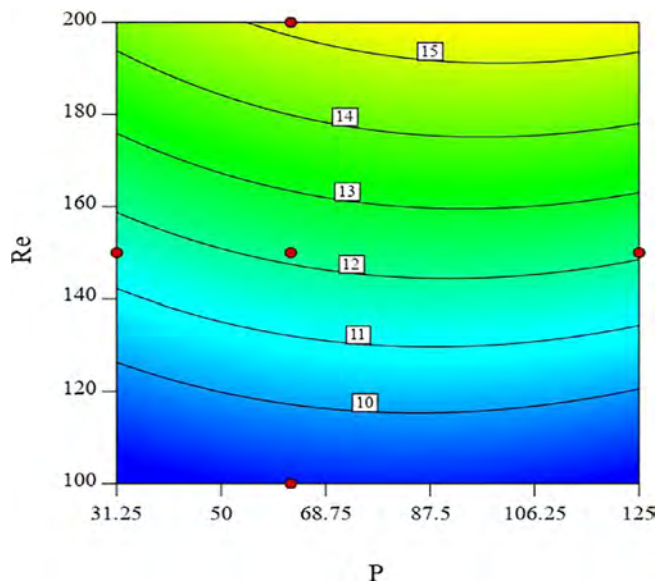


Fig. 19. Interactions of Reynolds number and stepping of Fins on the Nusselt number.

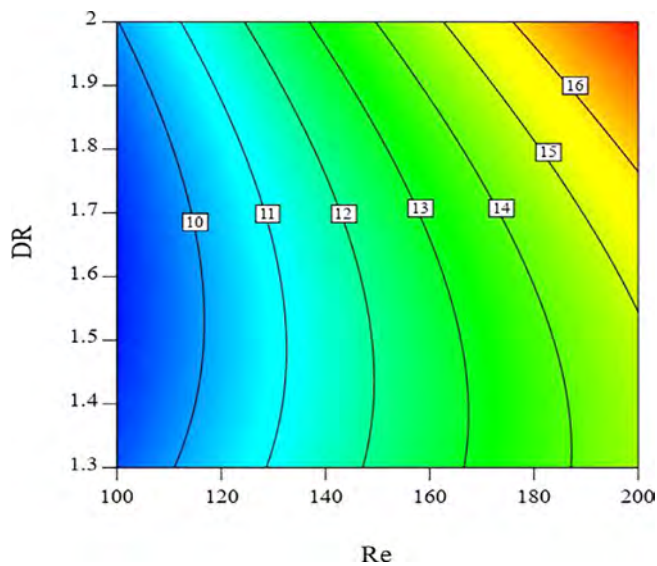


Fig. 20. Interactions of Reynolds number and diameter rate on the Nusselt number.

increasing the thickness of the Fins, the flow with high Reynolds passes out of the symmetric state and the vortices generated in the back of the Finns increase the Nusselt number.

The coefficient of friction is also considered as another goal. Given the relationship presented, this coefficient is directly related to the pressure drop which is undesirable and defined in optimizations as an undesirable goal and attempts to aim at reducing that coefficient. In Fig. 21, the interaction between the Reynolds number and the step on the coefficient of friction is considered. With increasing velocity, the coefficient of friction decreases, In other words, as it can be seen in diagram, the friction coefficient correlates with the Reynolds number

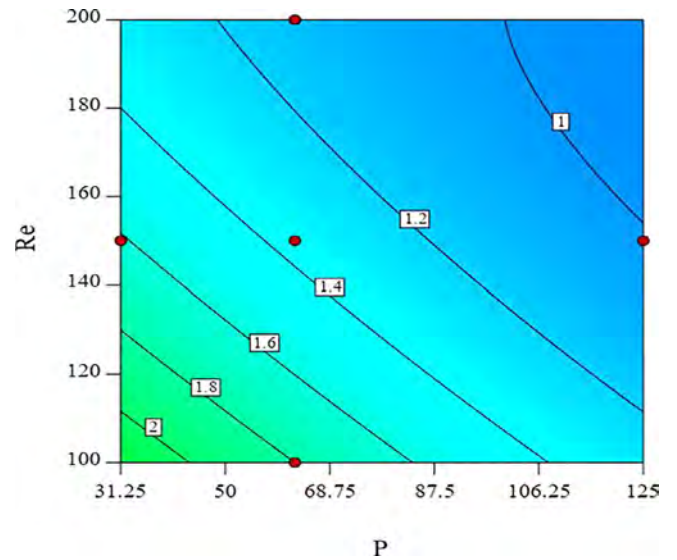


Fig. 21. Interaction of Reynolds number and stepping of fins on the Friction Coefficient.

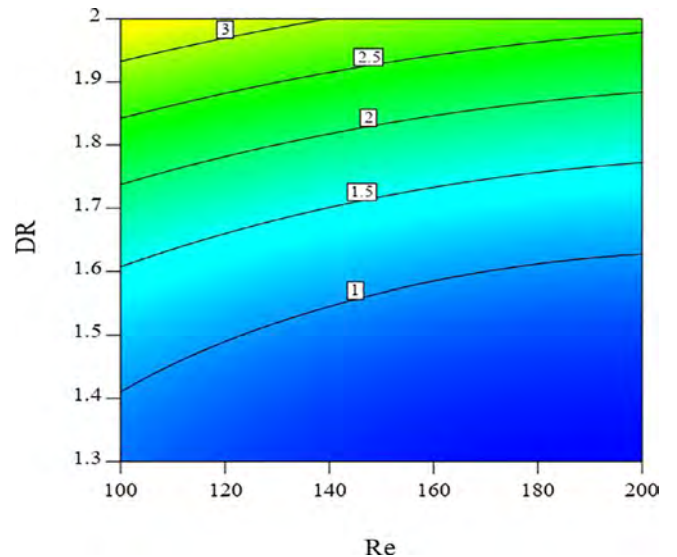


Fig. 22. interactions of Reynolds number and diameter rate on friction coefficient.

inversely. When the steps of fins are reduced or, in other words, the number of fins in the test area increases, the pressure drop increases and the coefficient of friction increases accordingly. The above items can be seen in the following figure.

By increasing the thickness of the Fins, the pressure drop in the BHE increases and this increase in pressure drop increases the friction coefficient. Fig. 22 shows the effect of the ring diameter rate as well as the Reynolds number on the coefficient of friction. When the Reynolds number is at its lowest value of 100 and the thickness of the Fin is in its highest state of 6.5 mm (DR = 2), we will have the highest coefficient of friction and pressure drop and this is Undesirable. The use of high-thickness Fins requires an increase in Reynolds number to reduce the

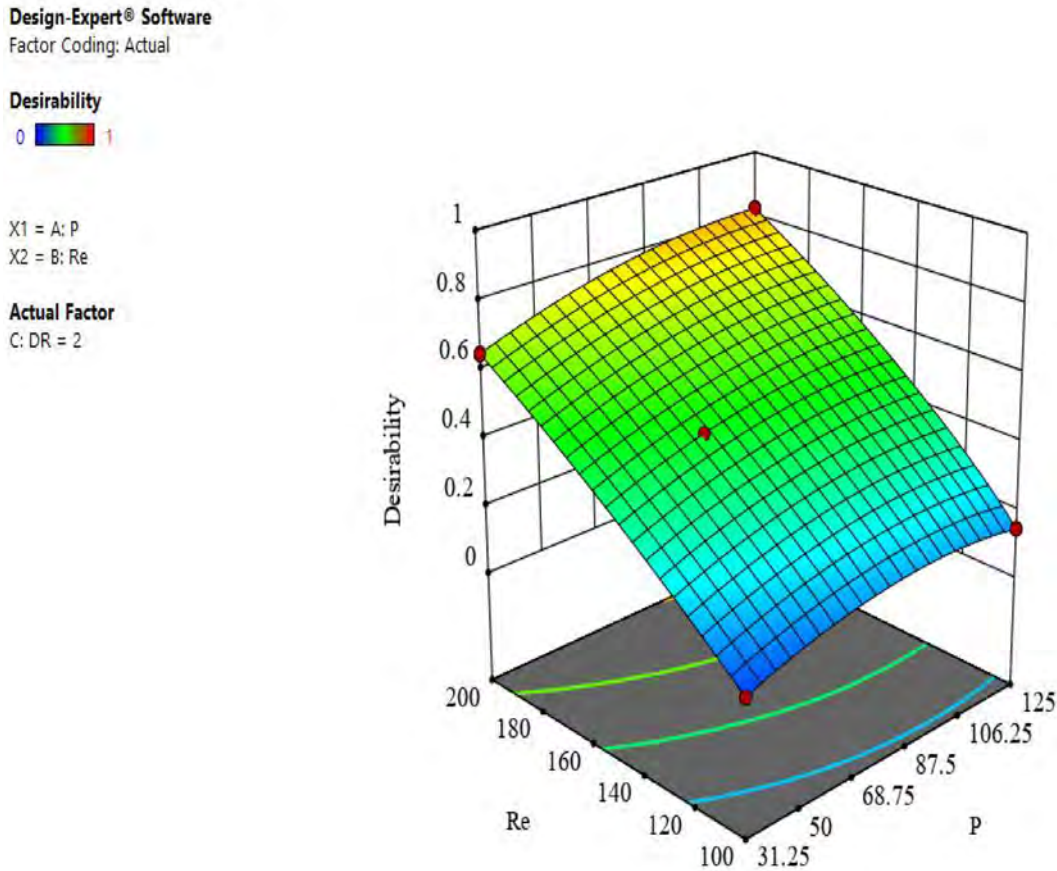


Fig. 23. The effect of Reynolds number and stepping of fins on optimization desirability.

impact of dropping pressure and increase overall system efficiency. It should be noted that the increase of the Reynolds number should be such that the flow is laminar. Desirability or accuracy in optimization is also considered in this article. Maximum accuracy of optimization using the response level method for the parameters studied is more than 80%. Interpretation of parameters on optimization desirability is presented in this section. In Fig. 23, the effect of Reynolds number and stepping of fins is shown in the form of a fixed value of the diameter rate on the optimization desirability. As can be seen, the best optimization desirability is observed. The desirability level of the design is shown in the figure above with respect to the other two parameters. The interaction between the step and the diameter rate parameters if the Reynolds is 200 is considered in Fig. 24. The interaction of these two parameters is less than the Reynolds number and the level of the characteristic is, as we see it, more uniform. But in any case, by increasing both parameters, a more optimal design can be achieved.

Also, in Fig. 25, the effect of the Reynolds number and the diameter rate on the optimization desirability is shown. If the step is 100, increasing the number of Reynolds and the diameter rate will increase the desirability of the plan. And in this case, high-efficiency designs can be achieved with respect to these two parameters.

In relations (11) and (12), with respect to optimization, the second degree relations of parameters for Nusselt number and coefficient of friction are presented. By setting different values of the parameters in

these relations, it can be obtained the mean value of Nusselt number and coefficient of friction.

$$Nu = -0.536348P^2 - 0.17332Re^2 + 0.76434DR^2 + 0.22051P \cdot Re + 0.02241P \cdot DR + 0.63164Re \cdot DR + 0.31545P + 3.25226Re + 0.94105DR \tag{11}$$

$$f = 0.94105P^2 + 0.10597Re^2 + 0.48672DR^2 + 0.12932P \cdot Re - 0.23022P \cdot DR - 0.10455Re \cdot DR - 0.30114P - 0.29105Re + 1.17658DR \tag{12}$$

Conclusion

In previous parts, temperatures distributions of single U-pipe, double U-pipe and centered inlet heat exchangers have been investigated. According to the contours and figures of three BHEs, it can be seen that a coaxial borehole heat exchanger with centered inlet has more performance compared to others. Also in optimization part, considering the design parameters and their result on the Nusselt number and friction coefficient, it was observed that the Reynolds number has the most effect among the parameters. As the Reynolds number increases, in addition to increasing heat transfer, the pressure drop will also decrease. The other two parameters have roughly the same value. By increasing the diameter rate and stepping distance, the

Design-Expert® Software
Factor Coding: Actual

Desirability
0  1

X1 = A: P
X2 = C: DR

Actual Factor
B: Re = 200

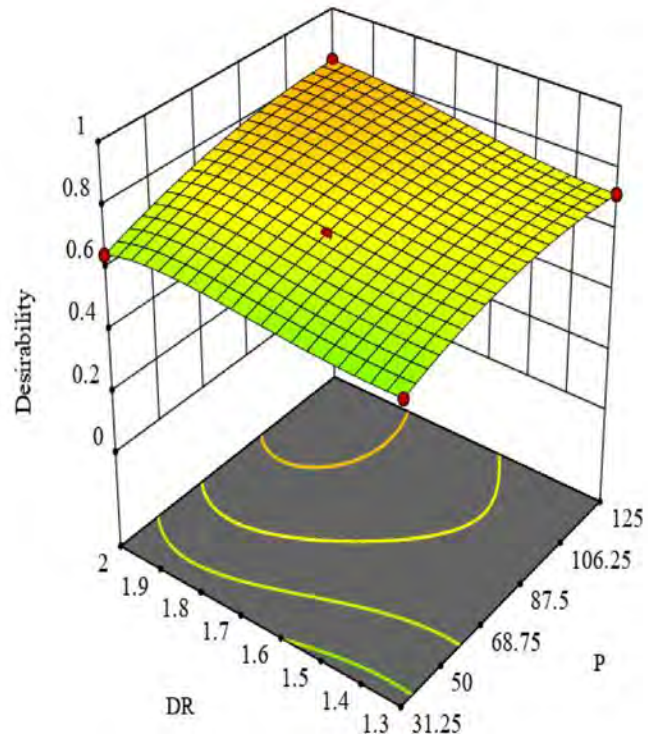


Fig. 24. The effect of diameter rate and stepping of fins on optimization desirability.

Design-Expert® Software
Factor Coding: Actual

Desirability
0  1

X1 = B: Re
X2 = C: DR

Actual Factor
A: P = 100

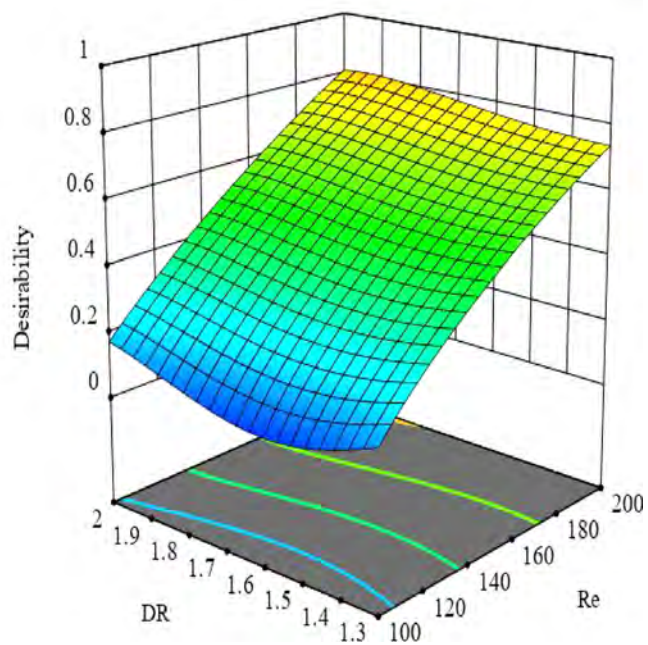


Fig. 25. The effect of diameter rate and Reynolds number on optimization desirability.

efficiency and design desirability will increase. According to these simulations two relations are presented to better understanding of parameters effect. Therefore, the paper presents best geometry for the highest heat transfer rate, and geometry with fin is also proposed to increase the heat transfer in borehole heat exchanger, which can be applied to engineering applications.

Appendix

Because of large number of the other figures, which are corresponded of the simulation numbers, which is listed in Table 3, we have shown in Appendix. In Fig. A1, which is number 2, like to the case number 1, the Reynolds number is 100 and the diameter rate is 1.3, but the step has increased in this case. The flow type is the same as in the first case, but due to the reduction in the number of fins, the pressure drop has also decreased.

Acknowledgment

The authors would like to thank anonymous reviewers for their constructive comments.

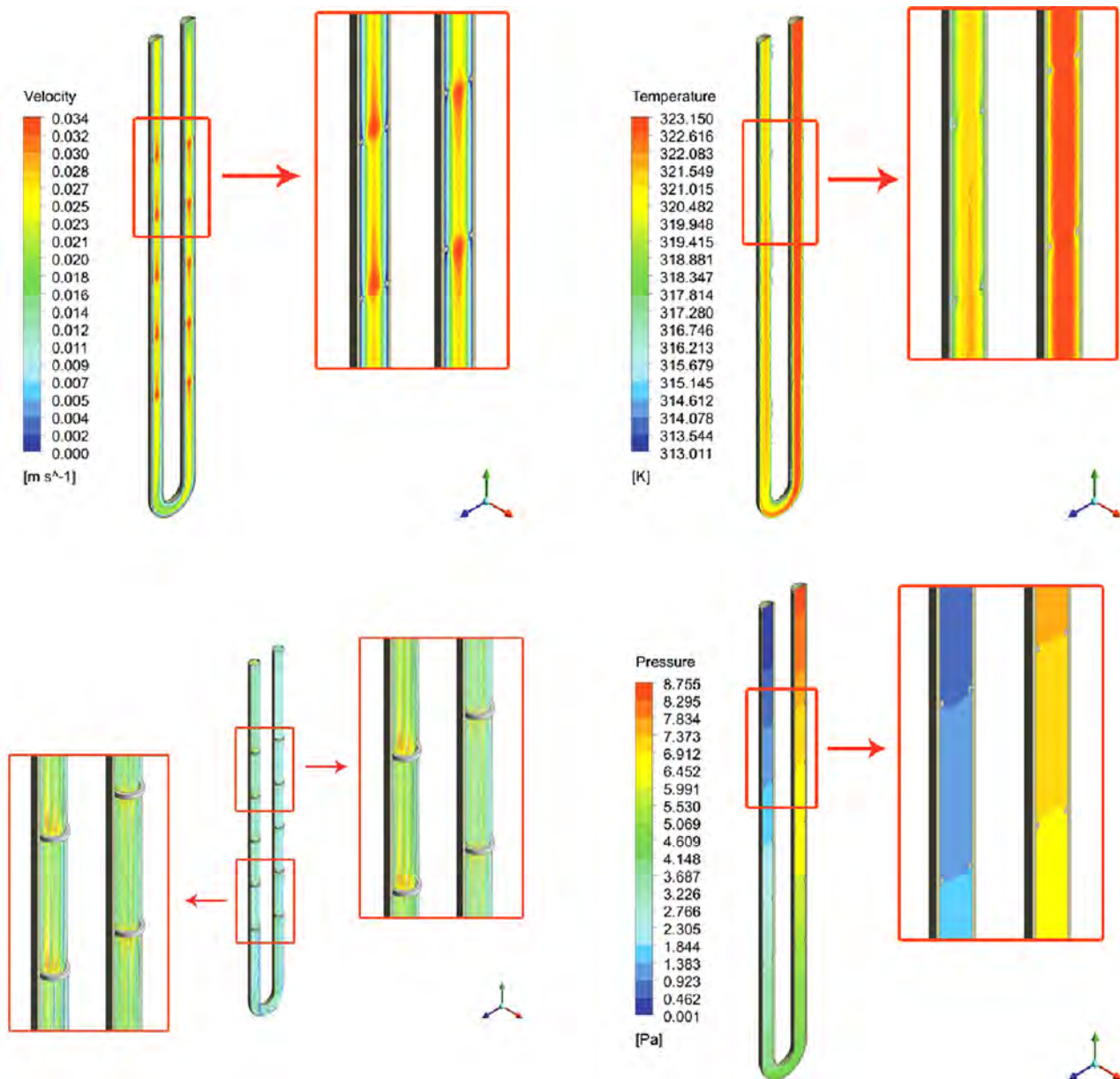


Fig. A1. Temperature, velocity, pressure and streamwise contours for case number 2.

Fig. A2 is also related to case number 3. In this case, the geometric parameters are the same as for case number 1, but the Reynolds number is in the amount of maximum. Due to the low thickness of the fins, the flow type is uniform but due to the high velocity, the fluid is less cooled and due to the difference in temperature between the fluid and the wall, which is more than number one, the result is more heat transfer. Case number 4 is like number 3, with the difference that the increased step as a result of the number of fins in test section is low (Fig. A3). In Fig. A4, the thickness of the Fin has been increased, but due to the Reynolds amount of 100, the fluid velocity is low and the flow is uniform. In this case, the step is 31.25 mm, and the difference with the first one is that the thickness of the fin is low (the diameter ratio of item number 1 is 1.3 and this case is 2). This is due to

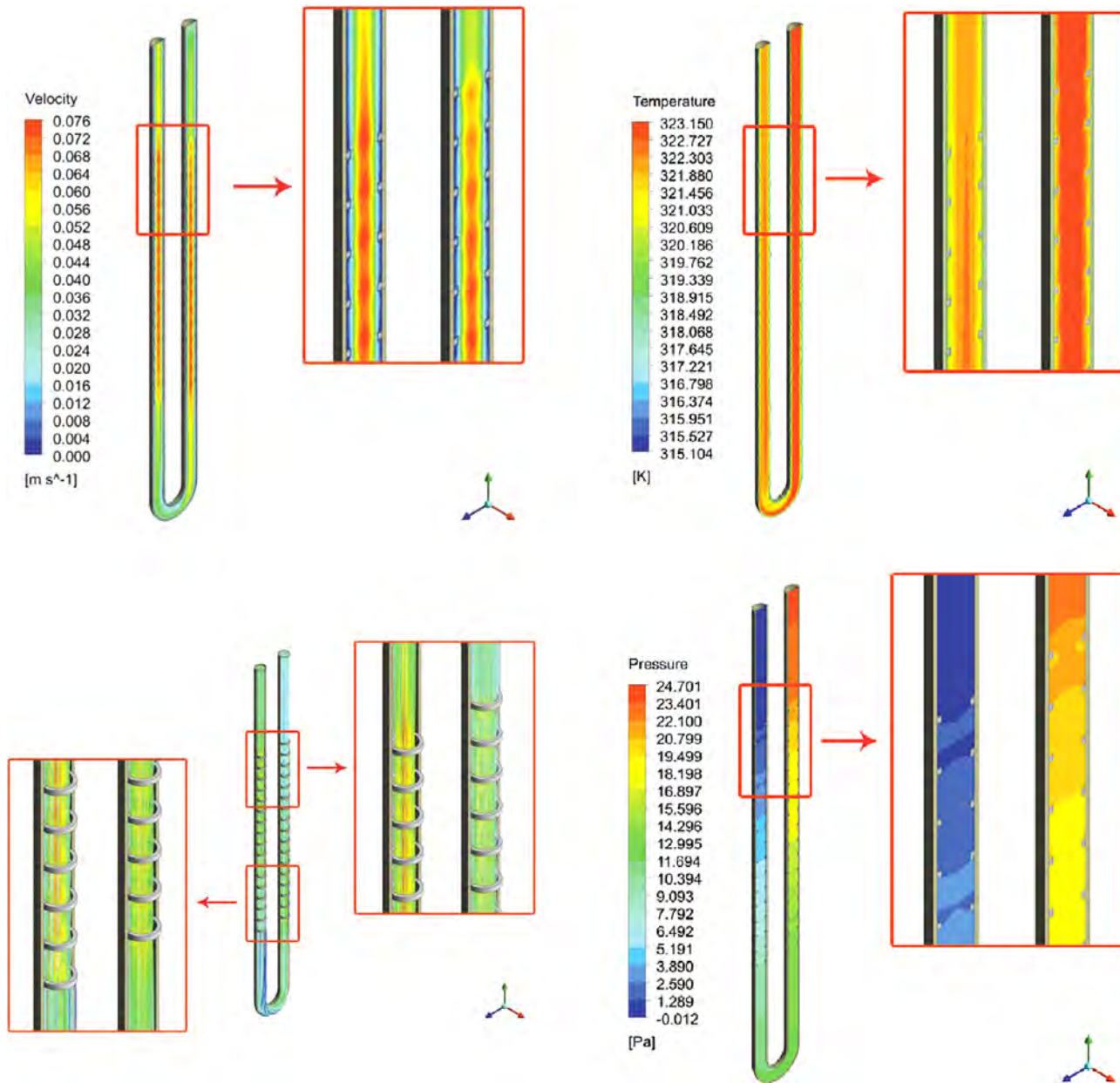


Fig. A2. Temperature, velocity, pressure and streamwise contours for case number 3.

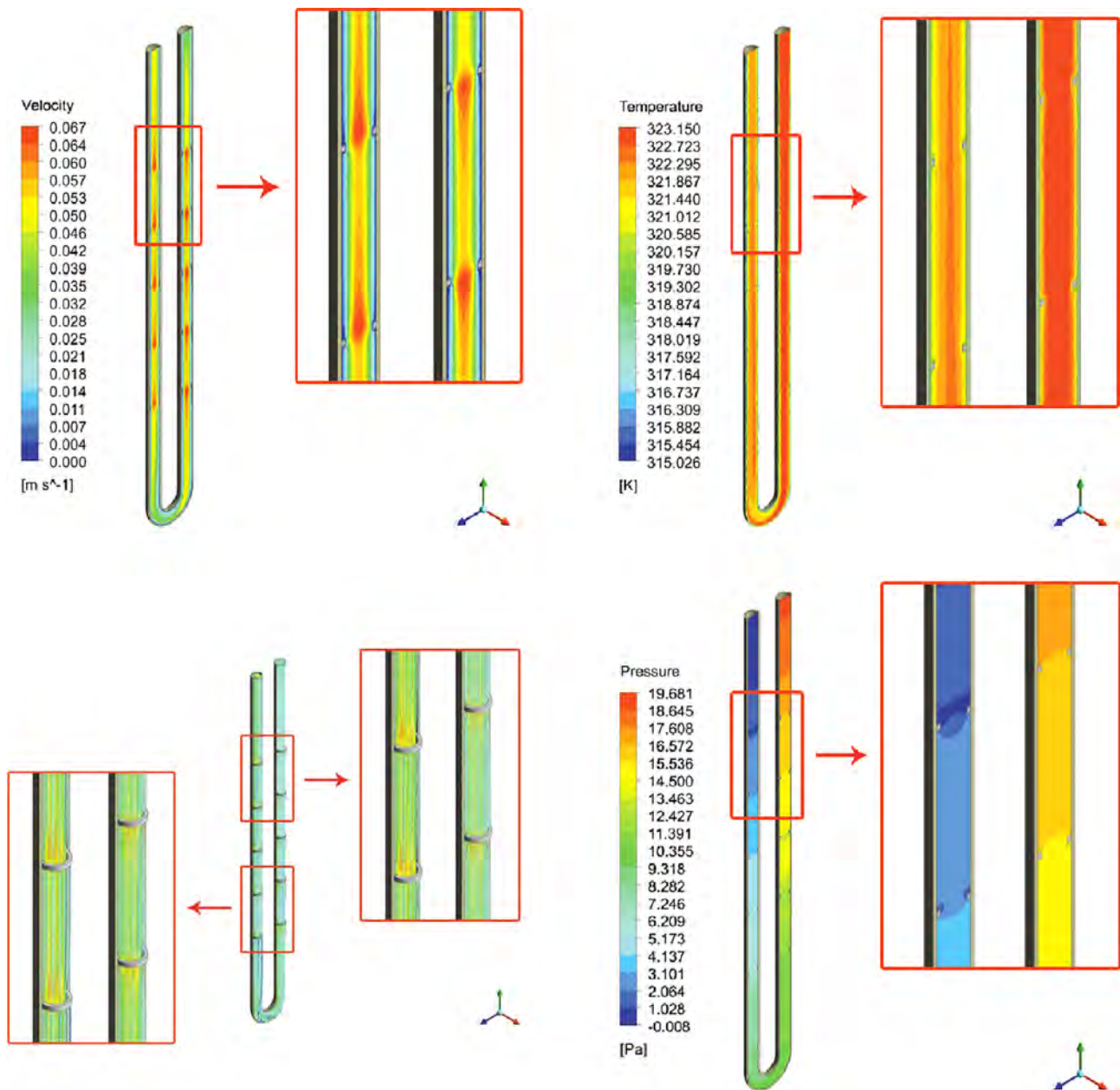


Fig. A3. Temperature, velocity, pressure and streamwise contours for case number 4.

the reduction of the cross-section at the edge of the fins, Reynolds It increases locally in that area and transfers more heat, which causes the flow to cool down. Fig. A5 shows the contours of item number 6. In this case, due to low Reynolds, the flow is uniform and due to the increase of the step, the pressure drop decreases. In the case of No. 7, considering the high Reynolds current and also the high Fin's thickness, after flow through the fins in the end, both the inlet region and the outlet region, a non-uniformity of the flow is observed (Fig. A6). The presence of this non-uniformity causes a sharp increase in the pressure drop, and is undesirable for the internal flow. In the optimization section, according to the figures shown, it can be seen that in such cases, due to the non-uniformity of the flow, the accuracy of the optimization has been reduced. Fig. A7 is also case number eight, in which case the step has been increased to number 7 and thus the pressure drop has decreased compared to that case.

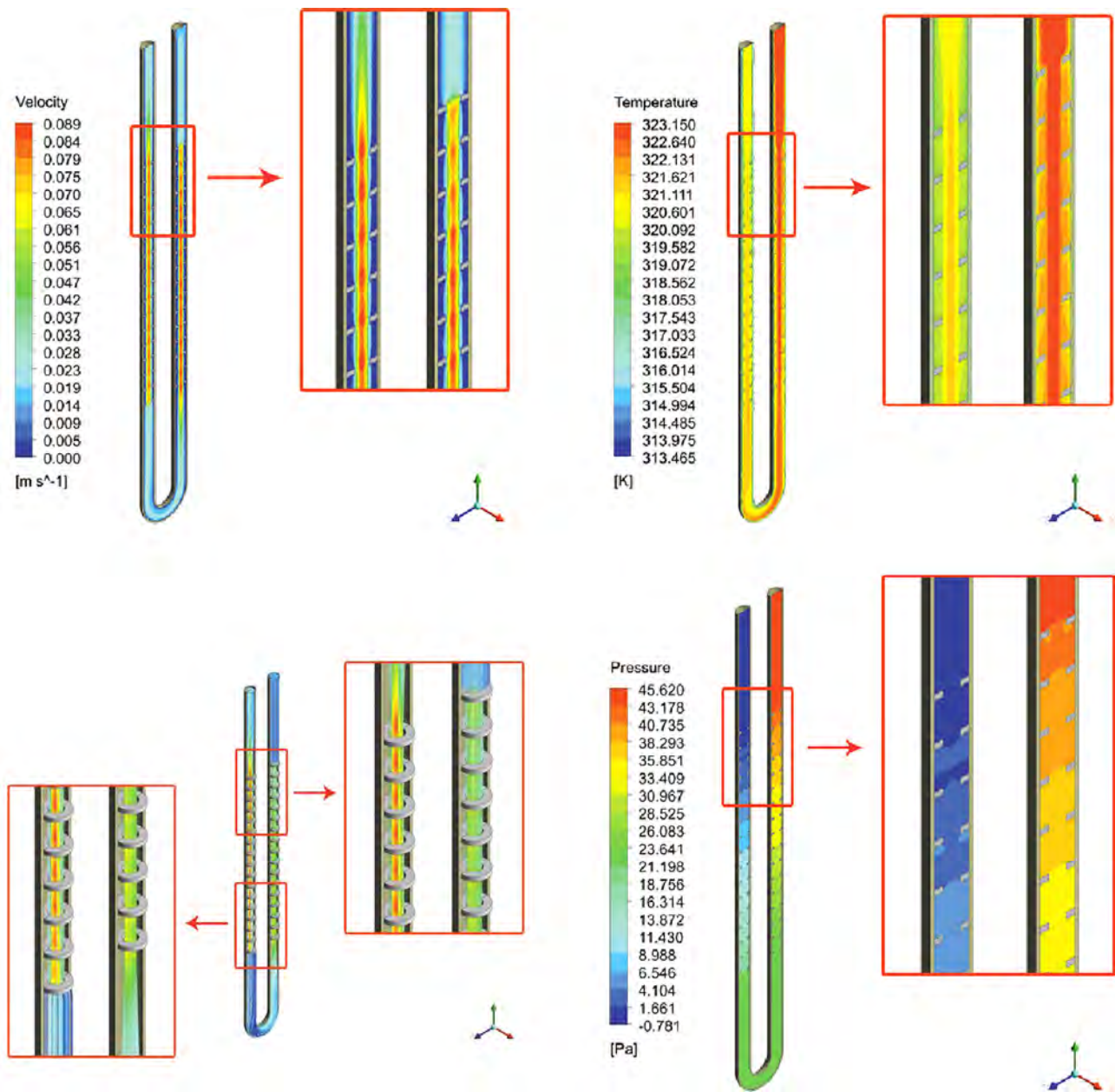


Fig. A4. Temperature, velocity, pressure and stream wise contours for case number 5.

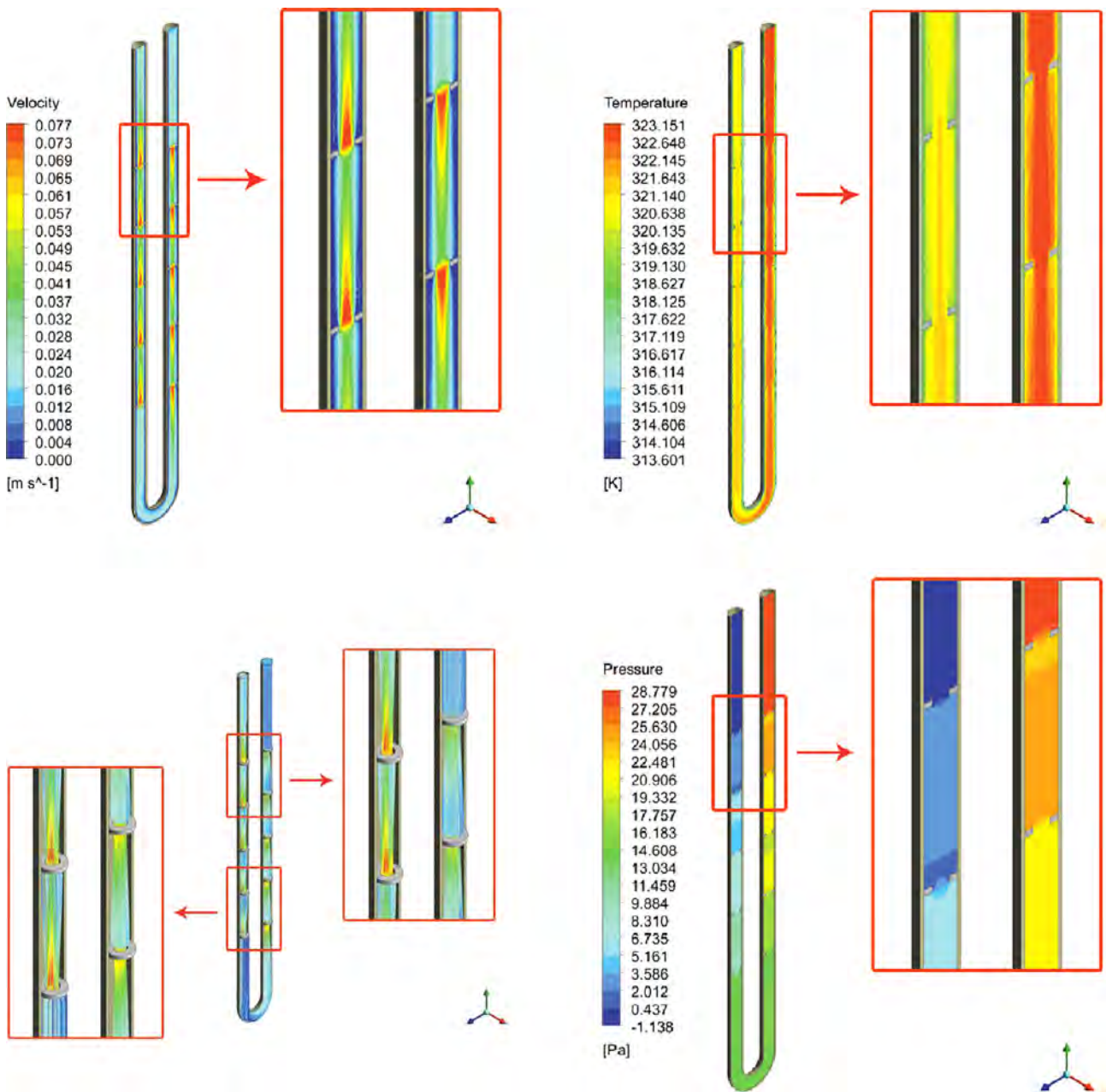


Fig. A5. Temperature, velocity, pressure and stream wise contours for case number 6.

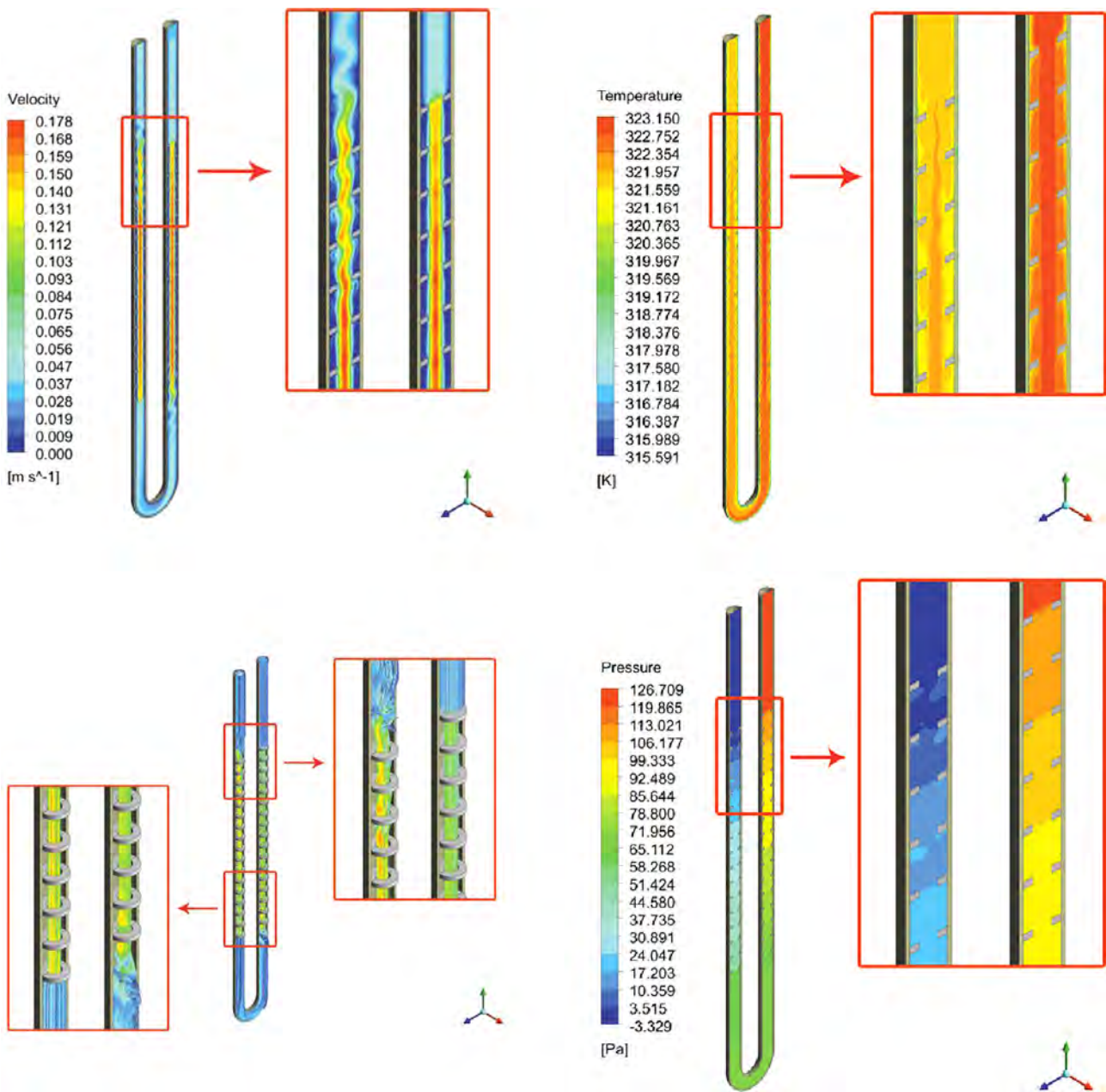


Fig. A6. Temperature, velocity, pressure and stream wise contours for case number 7.

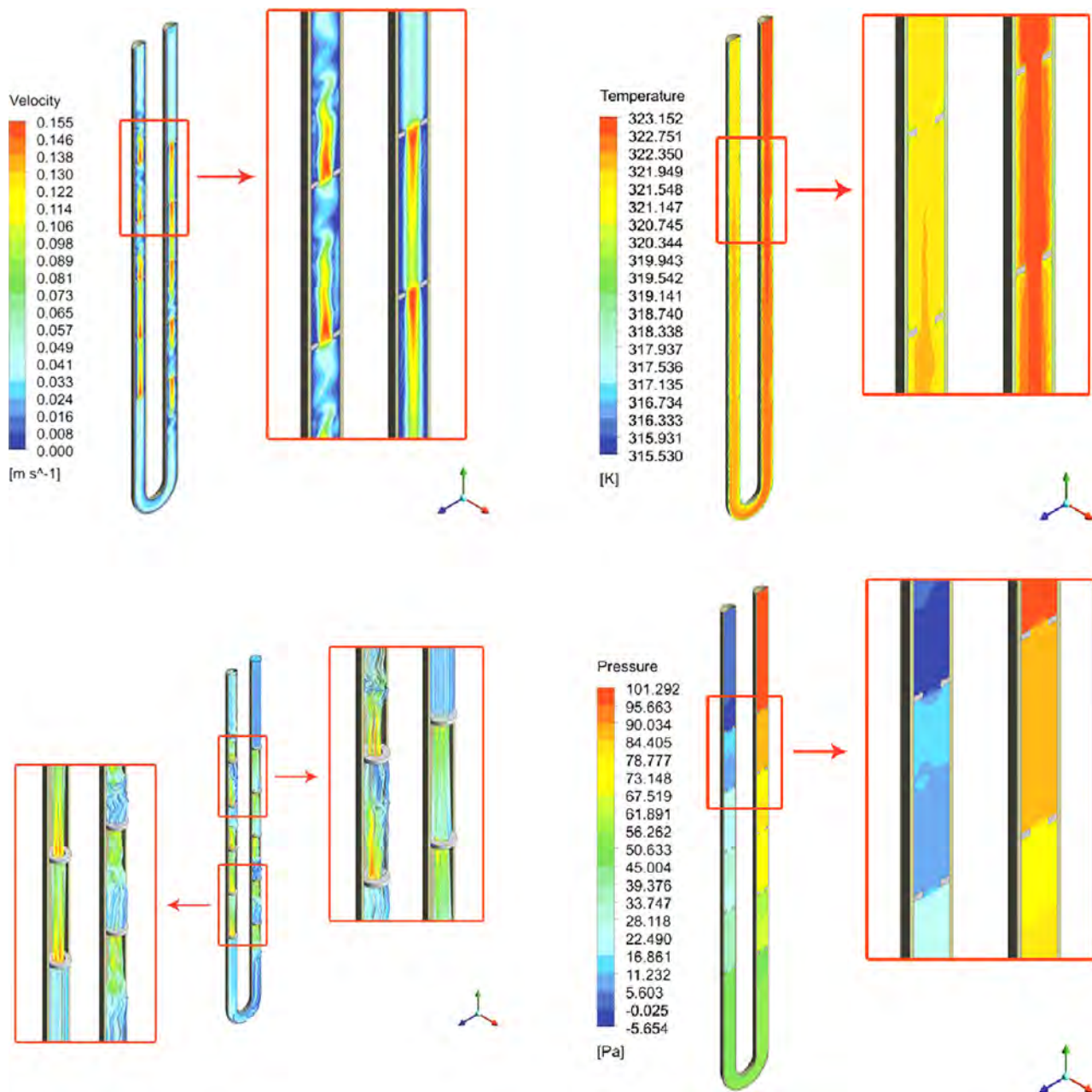


Fig. A7. Temperature, velocity, pressure and stream wise contours for case number 8.

References

- [1] Mogensen Palne. Fluid to duct wall heat transfer in duct system heat storages. Document-Swedish Council Build Res 1983;16:652–7.
- [2] ASHRAE, ASHRAE Handbook: HVAC Applications. ASHRAE, Atlanta, Georgia, USA; 2007. p. 12e15 [Chapter 32].
- [3] Sanner B, Hellström G, Spittler J, Gehlin S. Thermal response test—current status and world-wide application. In: Proceedings world geothermal congress 2005 Apr 24 (Vol. 200). International Geothermal Association.
- [4] Sheikholeslami M, Rashidi MM, Hayat T, Ganji DD. Free convection of magnetic nanofluid considering MFD viscosity effect. *J Mol Liq* 2016;218:393–9.
- [5] Sheikholeslami M, Ganji DD. Influence of electric field on Fe3O4- water nanofluid radiative and convective heat transfer in a permeable enclosure. *J Mol Liq* 2018;250:404–12.
- [6] Sheikholeslami Mohsen. Numerical simulation for solidification in a LHTESS by means of Nano-enhanced PCM. *J Taiwan Inst Chem Eng* 2018;86:25–41.
- [7] Florides G, Kalogirou S. Ground heat exchangers—A review of systems, models and applications. *Renewable Energy* 2007;32(15):2461–78.
- [8] Esen H, Inalli M, Esen M. Numerical and experimental analysis of a horizontal ground-coupled heat pump system. *Build Environ* 2007;42(3):1126–34.
- [9] Sheikholeslami M, Jafaryar M, Ganji DD, Li Zhixiong. Exergy loss analysis for nanofluid forced convection heat transfer in a pipe with modified turbulators. *J Mol Liq* 2018;262:104–10.
- [10] Li X, Chen Z, Zhao J. Simulation and experiment on the thermal performance of U-vertical ground coupled heat exchanger. *Appl Therm Eng* 2006;26(14):1564–71.
- [11] Karabacak R, Acar ŞG, Kumsar H, Gökgöz A, Kaya M, Tülek Y. Experimental investigation of the cooling performance of a ground source heat pump system in Denizli, Turkey. *Int J Refrigeration* 2011;34(2):454–65.
- [12] Michopoulos A, Kyriakis N. Predicting the fluid temperature at the exit of the vertical ground heat exchangers. *Appl Energy* 2009;86(10):2065–70.
- [13] Michopoulos AB, Bozis D, Kikidis P, Papakostas K, Kyriakis NA. Three-years operation experience of a ground source heat pump system in Northern Greece. *Energy Build* 2007;39(3):328–34.
- [14] Ozyurt O, Ekinci DA. Experimental study of vertical ground-source heat pump performance evaluation for cold climate in Turkey. *Appl Energy* 2011;88(4):1257–65.
- [15] Hwang Y, Lee JK, Jeong YM, Koo KM, Lee DH, Kim IK, et al. Cooling performance of a vertical ground-coupled heat pump system installed in a school building. *Renewable Energy* 2009;34(3):578–82.
- [16] Li XY, Li TY, Qu DQ, Yu JW. A new solution for thermal interference of vertical U-tube ground heat exchanger for cold area in China. *Geothermics* 2017;65:72–80.

- [17] Lei HY, Dai CS. Heat transfer analysis of centric borehole heat exchanger with different backfill materials. *Heat Transfer* 2015;19:25.
- [18] Crooijmans RA, Willems CJ, Nick HM, Bruhn DF. The influence of facies heterogeneity on the doublet performance in low-enthalpy geothermal sedimentary reservoirs. *Geothermics* 2016;64:209–19.
- [19] BniLam N, Al-Khoury R. A spectral element model for nonhomogeneous heat flow in shallow geothermal systems. *Int J Heat Mass Transf* 2017;104:703–17.
- [20] Akbar S, Fathianpour N, Al Khoury R. A finite element model for high enthalpy two-phase flow in geothermal wellbores. *Renewable Energy* 2016;94:223–36.
- [21] Al-Khoury Rafid. Computational modeling of shallow geothermal systems. CRC Press; 2011.
- [22] Javed S, Claesson J. New analytical and numerical solutions for the short-term analysis of vertical ground heat exchangers. *ASHRAE Trans* 2018;117(1):3.
- [23] Sheikholeslami M, Jafaryar M, Li Zhixiong. Nanofluid turbulent convective flow in a circular duct with helical turbulators considering CuO nanoparticles. *Int J Heat Mass Transfer* 2018;124:980–9.
- [24] Sheikholeslami M, Jafaryar M, Saleem S, Li Zhixiong, Shafee Ahmad, Jiang Yu. Nanofluid heat transfer augmentation and exergy loss inside a pipe equipped with innovative turbulators. *Int J Heat Mass Transfer* 2018;126:156–63.
- [25] Javed S, Fahlén P, Claesson J. Vertical ground heat exchangers: a review of heat flow models. In *Effstock 2009-Stockholm, Sweden, 2009-06-14–17. Proceedings vol. CD-proceedings*; 2009.
- [26] Al-Khoury Rafid. Spectral framework for geothermal borehole heat exchangers. *Int J Numer Meth Heat Fluid Flow* 2010;20(7):773–93.